Proteins as Solvents: The Role of Amino Acid Composition in the Excited-State Charge Transfer Dynamics of Plastocyanins

G. R. Loppnow* and E. Fraga

Contribution from the Department of Chemistry, University of Alberta, Edmonton, Alberta, Canada T6G 2G2

Received August 26, 1996[⊗]

Abstract: The resonance Raman intensities for parsley, spinach, and poplar *a* plastocyanins, blue copper proteins involved in plant photosynthetic electron transport, have been measured at wavelengths throughout the S(Cys) → Cu charge transfer absorption band centered at 597 nm in an effort to determine the role of amino acid composition on the dynamics of excited-state charge transfer. The resonance Raman spectra of the three plastocyanins exhibit vibrational bands with similar frequencies but different relative intensities. Self-consistent analysis of the absorption band and resulting resonance Raman excitation profiles for each of the plastocyanins demonstrates that many of the derived molecular parameters are similar, including the zero−zero energy, the transition moment, and the homogeneous and inhomogeneous linewidths. However, significant differences are observed in the mode-specific excited-state geometry distortions even though the total, mode-specific reorganization energy obtained from the resonance Raman intensities of specific vibrations is 0.18 ± 0.01 eV for all three plastocyanins. A detailed comparison of the structural and electrostatic differences in spinach and poplar *a* plastocyanin using the previously reported structure of poplar *a* plastocyanin, potential energy minimization, and calculation of the electrostatic field with the linearized Poisson−Boltzmann equation suggests that the mode-specific relative intensity differences arise from a change in the normal mode description due to differential coupling of internal coordinates localized on amino acid residues at least 8 Å from the copper site. These results demonstrate that the protein environment is strongly coupled to the copper site and that a significant portion of the protein, which is not involved in binding of redox partners, determines the copper site coordination geometry and resulting redox potential. An important result is that the mode-specific protein component of the reorganization energy on the 20 fs time scale is sensitive to protein composition differences that are at least 8 Å from the charge transfer site.

Introduction

The rate constant for electron transfer in proteins can be related to a number of factors by the Marcus equation:[1−4] $k_{ET} \propto \exp\{-(\Delta G^\circ + \lambda)^2/4\lambda RT\} \exp\{-\beta(r - r_0)\}$ where ΔG° is the free energy change upon electron transfer, λ is the reorganization energy, r is the distance between donor and acceptor, and β is an empirical constant reflecting the distance dependence of electron transfer. The reorganization energy is usually written as the sum of the inner and outer sphere contributions ($\lambda = \lambda_i + \lambda_o$), where λ_i is loosely defined as the structural reorganization of the donor and acceptor (nuclear) conformation, and λ_o is defined as the structural reorganization of the solvent (electronic and nuclear) conformation to the new electronic distribution. Although measurements of total reorganization energies in a number of systems have been made, the contributions of individual molecular motions to the reorganization energy, particularly those of the solvent, have been difficult to determine, producing an inadequate molecular picture of the role of structure and dynamics in electron and charge transfer.

Resonance Raman intensities provide detailed information about excited-state structure and dynamics on an extremely fast time scale.[5] By tuning the exciting laser into an absorption band, such as a charge transfer band, resonant enhancement of those normal modes coupled to the electronic excitation occurs; the resonance Raman intensities directly reflect the conformational distortion of the molecule along each normal mode upon excitation to an electronic excited state. Measurement of the resonance Raman intensity of each vibration as a function of excitation wavelength within an absorption band yields a set of resonance Raman excitation profiles. Self-consistent analysis of the resonance Raman excitation profiles and the absorption spectrum can yield such molecular parameters as the distortion along each normal mode upon photoexcitation, excited-state lifetime, and transition moment.[5]

In a previous paper,[6] we determined the excited-state photophysics of charge transfer in parsley plastocyanin, a 10 500 Da copper protein that acts as an electron transport agent between cytochrome *f* and photosystem I in plant photosynthesis,[7] by using the resonance Raman intensities, fluorescence spectrum, and absorption spectrum. Plastocyanin was used because the structure of the protein is well established[8] and because the copper ion is buried among hydrophobic amino acid residues in one end of the protein and does not show any solvent accessibility.[8,9] It was found that the protein environment contributes to the total reorganization energy in two ways, a

* To whom correspondence should be addressed. E-Mail: glen.loppnow@ualberta.ca.

[⊗] Abstract published in *Advance ACS Abstracts,* January 15, 1997.

(1) Marcus, R. A.; Sutin, N. *Biochim. Biophys. Acta* **1985**, *811*, 265.
(2) McLendon, G.; Hake, R. *Chem. Rev.* **1992**, *92*, 481.
(3) Natan, M. J.; Baxter, W. W.; Kuila, D.; Gingrich, D. J.; Martin, G. S.; Hoffman, B. M. In *Electron Transfer in Inorganic, Organic, and Biological Systems*; Bolton, J. R., Mataga, M., McLendon, G., Eds.; American Chemical Society: Washington, DC, 1991; p 201.
(4) Winkler, J. R.; Gray, H. B. *Chem. Rev.* **1992**, *92*, 369.
(5) Myers, A. B.; Mathies, R. A. In *Biological Applications of Raman Spectroscopy*; Spiro, T. G., Ed.; Wiley: New York, 1988; Vol. 2, p 1.
(6) Webb, M. A.; Fraga, E.; and Loppnow, G. R. *J. Phys. Chem.* **1996**, *100*, 3278.
(7) Sykes, A. G. *Chem. Soc. Rev.* **1985**, *14*, 283.
(8) Guss, J. M.; Freeman, H. C. *J. Mol. Biol.* **1983**, *169*, 521.
(9) Boden, N.; Holmes, M. C.; Knowles, P. F. *Biochem. Biophys. Res. Commun.* **1974**, *57*, 845.

S0002-7863(96)02983-6 CCC: $14.00

mode-specific component in the resonance-enhanced vibrations and a bulk solvent-like dephasing component as evidenced by the homogeneous linewidth.[6]

In this paper, we examine more closely the role of environment on excited-state processes by comparing the excited-state charge transfer dynamics in parsley, spinach, and poplar *a* plastocyanin. The primary goal of this work was to determine the mode-specific charge transfer dynamics in a model system in which the charge transfer complex has a well-defined structure and sits in a relatively isolated, well-characterized environment. Because of the lack of solvent accessibility in plastocyanin, the protein plays the role of the solvent. In this paper, we have used absorption and resonance Raman spectroscopy of the three plastocyanins, which have slightly different amino acid compositions, to measure the mode-specific reorganization energies upon charge transfer along each of the observed normal modes. Comparison of the derived molecular distortions upon charge transfer demonstrates a mode-specific difference in excited-state dynamics among the three plastocyanins, although the total reorganization energy remains constant. These results are discussed with respect to the ground-state normal modes, excited-state distortions, and electrostatic environment of plastocyanin. An important result is that the mode-specific protein component of the reorganization energy on the 20 fs time scale is sensitive to protein composition differences that are at least 8 Å from the charge transfer site.

Experimental Section

Protein Purification. Plastocyanin was isolated from poplar, parsley, and spinach leaves according to literature procedures with slight modifications.[10,11] Parsley and spinach leaves were obtained commercially, and poplar leaves were obtained from local trees. The isolation and purification of poplar *a* plastocyanin is identical to that of parsley, described earlier.[6] For spinach plastocyanin,[12] the isolation and purification procedure was slightly different. Briefly, 5 kg of spinach leaves, in 1 kg batches, were homogenized with 1.2 L of a sucrose buffer (0.4 M sucrose, 50 mM KCl, 50 mM TRIS−HCl, pH 8.0). The homogenate was squeezed through plain cloth and centrifuged. The chloroplast pellet was resuspended in TRIS−HCl (500 mM TRIS−HCl, pH 8.0) to a final volume of 400 mL. Cold acetone was added slowly with vigorous stirring to a final concentration of 35% (v/v). After stirring and centrifugation, the supernatant was diluted with acetone to a final concentration of 80% (v/v) to precipitate plastocyanin. The precipitate was allowed to settle for 1−2 h, and the precipitate collected by decantation. The sediment was collected by centrifugation, mixed with the smallest possible volume (∼300 mL) of 60 mM TRIS−HCl (pH 7.6), and dialyzed against 60 mM TRIS−HCl (pH 7.6). After centrifugation, the supernatant was purified on DEAE-cellulose and Sephadex G-50 columns. A second DEAE-cellulose and/or Sephadex G-50 column was sometimes used to further purify the plastocyanin. Typical yields of plastocyanin were 16−28 mg for parsley, 29−40 mg for poplar, and 3−10 mg for spinach per kilogram of leaves. The purity of plastocyanin was determined by the A_{278}/A_{597} ratio and was 1.6 for parsley, 1.1 for poplar, and 1.4 for spinach. The difference in purity ratios reflects the different aromatic amino acid compositions of the three proteins.[7]

Resonance Raman Spectroscopy. Plastocyanin samples for the resonance Raman and fluorescence experiments were prepared by quantitative dilution of plastocyanin (50 mM TRIS−HCl, pH 7.6) with a cacodylate/TRIS buffer solution (0.5 M cacodylic acid, 50 mM TRIS−HCl, pH 7.6). The cacodylate/TRIS buffer solution was made fresh every week because of slight decomposition on this time scale. The addition of cacodylate provided an internal intensity standard and did not have a noticeable effect on the absorption or resonance Raman spectra of plastocyanin. Room-temperature resonance Raman spectra of plastocyanin were obtained with 300 μL sample solutions having an absorbance of 5−7 OD/cm at 597 nm (ϵ = 4500 M^{-1} cm^{-1})[7]. Resonance Raman scattering was excited by spherically focusing the laser onto a spinning 5 mm o.d. NMR tube containing the sample solution in a 135° back-scattering geometry. Laser excitation was obtained with Kr and Ar ion lasers (Coherent, Santa Clara, CA) and HeNe lasers (PMS Electro-Optics, Boulder, CO). The wavelengths used were 514.5, 530.9, 568.2, 594, 612, and 647.1 nm. The laser power was 60−100 mW (Kr and Ar ion lasers) or 7 mW (HeNe lasers). Multichannel detection of the resonance Raman scattering was obtained with a liquid nitrogen-cooled CCD detector (Princeton Instruments, Trenton, NJ) connected to the first half of a double monochromator (Spex Industries, Metuchen, NJ). Spectral slit widths were 5−7 cm^{-1}. Frequency calibration was done by measuring Raman scattering of solvents of known frequencies (benzene, chloroform, and carbon tetrachloride). Reported frequencies are accurate to ±2 cm^{-1}. Absorption spectra were measured by using a diode array spectrophotometer (Hewlett-Packard, Sunnyvale, CA).

The resonance Raman spectra were analyzed by subtracting a buffer solution (50 mM TRIS−HCl, pH 7.6) background from all spectra. The spectra were corrected for the wavelength dependence of the spectrometer efficiency by dividing the background-subtracted resonance Raman spectra by the measured spectrum of a standard lamp (Electro Optics Associates, Palo Alto, CA) and multiplying the resulting spectrum by the standard lamp spectral output. The baselines were leveled by subtracting multiple joined line segments from the spectrum. Spectra were smoothed using a 5-point Savitsky−Golay function. Intensities of plastocyanin relative to the 603 + 638 cm^{-1} lines of cacodylate were measured by integration of peak areas. Overlapping peaks were separated by fitting regions of the spectra to sums of Lorentzian/Gaussian peaks. To minimize errors in the fitting of overlapped peaks, the frequencies and band widths of the peaks were fixed to the same values for the spectra of each species at all excitation wavelengths; only the heights of the peaks were allowed to vary. Bleaching of the sample was corrected by measuring the absorbance at 700 nm (ϵ = 1295 M^{-1} cm^{-1}) before and after each scan, and the average absorbance was used to determine the plastocyanin concentration. This procedure has previously been shown to be reasonable for plastocyanin due to the low bulk photoalteration parameter.[6] Measurement of the resonance Raman spectrum and determination of the intensities were repeated on 3−9 fresh samples of plastocyanin for each wavelength.

The methods used here for converting the resonance Raman intensities of plastocyanin into absolute cross-sections and for correcting for self-absorption effects have been described previously.[6] The cross-sections of cacodylate used in the determination of absolute cross-sections were also determined previously.[6]

Molecular Modeling. All calculations were performed on an Indigo^2 workstation (Silicon Graphics Inc., Palo Alto, CA) using the InsightII molecular modeling environment software containing the Biopolymer, DelPhi, and Discover modules (Molecular Simulations, Inc., Palo Alto, CA). Atomic coordinates for poplar *a* plastocyanin[13] were obtained from the Brookhaven Protein Data Bank.[14] The following procedure was used to generate the structure of spinach plastocyanin. The structure of poplar *a* plastocyanin was used as the starting point for the structure of spinach plastocyanin due to the high (78%) degree of homology between the two proteins.[15] The amino acids of poplar *a* plastocyanin were "mutated" to those of spinach plastocyanin by using the Biopolymer module of InsightII. The new amino acids were constrained to lie along the coordinates of the old amino acids as much as was feasible. The poplar *a* plastocyanin structure from the X-ray coordinates and the mutated poplar *a* plastocyanin structure (spinach plastocyanin) were then minimized by

(10) Plesnicar, M.; Bendall, D. S. *Biochim. Biophys. Acta* **1970**, *216*, 192.
(11) Graziani, M. T.; Agro, A. F.; Rotilio, G.; Barra, D.; Mondovi, B. *Biochemistry* **1974**, *13*, 804.
(12) Morand, L. Z; Krogmann, D. W . *Biochim. Biophys. Acta* **1993**, *1141*, 105.
(13) Guss, J. M.; Bartunik, H. D.; Freeman, H. C. *Acta Crystallogr.* **1992**, *B48*, 790.
(14) Bernstein, F. C.; Koetzle, T. F.; Williams, G. J. B.; Meyer, E. F., Jr.; Brice, M. D.; Rodgers, J. R.; Kennard, O.; Shimanouchi, T.; Tasumi, M. *J. Mol. Biol.* **1977**, *112*, 535.
(15) Sykes, A. G. *Adv. Inorg. Chem.* **1991**, *36*, 377.

using the AMBER[16,17] force field with the Discover software. This approach permits a comparison between the two structures while minimizing the systematic errors introduced by the choice of energy minimization force field and parameters. Energy minimization proceeded by using the methods of steepest descent and conjugated derivative by the Newton−Raphson algorithm until the calculated energy gradient was ≤ 0.001 kcal mol^{-1} along each coordinate. A distance-dependent dielectric was assumed in which $\epsilon = 4r$ and r is the distance from the center of the protein in Å. The distance-dependent dielectric has been shown by others to effectively model the bulk solvent and dielectric effects in proteins.[18−21] In the program, 1−4 nonbonded interactions were scaled by 0.5.

Calculation of the electrostatic potential in the protein was performed by using the finite difference solutions to the linear Poisson−Boltzmann equation[22] as implemented in the DelPhi[23,24] module of InsightII. The linear Poisson−Boltzmann equation is[22−25]

$$\nabla\epsilon(r)\nabla\Phi(r) - \epsilon\kappa^2\Phi(r) = -4\pi\rho^{\mathrm{f}}(r)/kT \qquad (1)$$

where $\epsilon(r)$ is the position-dependent dielectric permittivity, $\Phi(r)$ is the potential, $\rho^{\mathrm{f}}(r)$ is the fixed charge density, $\kappa = (8\pi e^2 N_{\mathrm{A}} I/1000kT)^{1/2}$ is the Debye−Hückel inverse length, N_{A} is Avogadro's number, I is the ionic strength, k is Boltzmann's constant, and T is the temperature. In the finite difference method, the linear Poisson−Boltzmann equation is replaced by a series of finite difference equations solved iteratively. In the DelPhi software package, the solvent and protein coordinates are mapped on a three-dimensional grid. Each grid point is assigned a value for the charge, dielectric constant, and ionic strength. Boundary conditions are set by the Coulomb equation. For plastocyanin, a low dielectric (2) was assigned to the protein and a high dielectric (80) was assigned to the region outside the protein, assumed to be a dielectric continuum. The ionic strength was assumed to be 0, effectively removing the second term in eq 1. The standard DelPhi protein formal charges, in which 1−2 atoms of each amino acid residue carry the total formal charge at physiological pH for that residue, were used for plastocyanin. The calculations were set up with 65 grid points for each dimension and a minimum 15 Å border space between the edge of the protein and the edge of the box.

Theory. The absorption and resonance Raman cross-sections in the Condon approximation can be written using the time dependent formalism of Lee and Heller:[5,26]

$$\sigma_{\mathrm{A}} = \frac{4\pi E_{\mathrm{L}} e^2 \mathrm{M}^2}{6\hbar^2 cn} \int_{-\infty}^{\infty} \mathrm{d}E_0\, H(E_0) \int_{-\infty}^{\infty} \mathrm{d}t\, \langle i|i(t)\rangle \exp\left\{\frac{i(E_{\mathrm{L}} + \epsilon_{\mathrm{i}})t}{\hbar}\right\} G(t) \qquad (2)$$

$$\sigma_{\mathrm{R}} = \frac{8\pi E_{\mathrm{S}}{}^3 E_{\mathrm{L}} e^4 \mathrm{M}^4}{9\hbar^6 c^4} \int_{-\infty}^{\infty} \mathrm{d}E_0\, H(E_0) \left| \int_0^{\infty} \mathrm{d}t\, \langle f|i(t)\rangle \times \exp\left\{\frac{i(E_{\mathrm{L}} + \epsilon_{\mathrm{i}})t}{\hbar}\right\} G(t) \right|^2 \qquad (3)$$

where E_{L} and E_{S} are the energies of the incident and scattered photons, respectively, n is the refractive index, M is the transition length, ϵ_{i} is the energy of the initial vibrational state, $|i\rangle$ and $|f\rangle$ are the initial and final vibrational wave functions, $H(E_0)$ is a normalized inhomogeneous distribution of site electronic energies (usually assumed to be Gaussian), $G(t)$ is the homogeneous linewidth function, and $|i(t)\rangle = \mathrm{e}^{-iHt/\hbar}|i\rangle$ is the initial ground vibrational wave function propagated on the excited electronic state potential surface. The processes represented by these two equations are shown in Figure 1. In absorption, the incident photon carries the ground-state vibrational wave function to the excited electronic state where it propagates under the influence of the excited-state Hamiltonian. As it propagates, the amplitude of the wavepacket and phase coherence of the basis wave functions making up the wavepacket decay through population relaxation and dephasing processes, respectively. These decay processes are represented in eqs 2 and 3 by $G(t)$. Thus, the absorption cross-section is simply the Fourier transform of the overlap between the initial state and the propagating initial state on the excited electronic state potential surface along each normal coordinate of the molecule, multiplied by the decay function $G(t)$. Similarly, the resonance Raman cross-section is simply the square of the half Fourier transform of the overlap between the final state and the propagating initial state on the excited electronic state potential surface along each normal coordinate multiplied by the decay function $G(t)$. The $\langle i|i(t)\rangle$ absorption overlap in eq 2 is the product of one-dimensional $\langle i|i(t)\rangle$ overlaps for each normal mode, and the $\langle f|i(t)\rangle$ Raman overlap in eq 3 is the product of $\langle f|i(t)\rangle$ along the Raman-active mode and $\langle i|i(t)\rangle$ along all other modes. In this treatment, the $\langle i|i(t)\rangle$ and $\langle f|i(t)\rangle$ overlaps are dependent only on the displacement, Δ, in dimensionless normal coordinates between ground- and excited-state equilibrium geometries along each normal coordinate. The general implementation of these equations have been described in detail,[5,27,28] as has their specific application to parsley plastocyanin.[6]

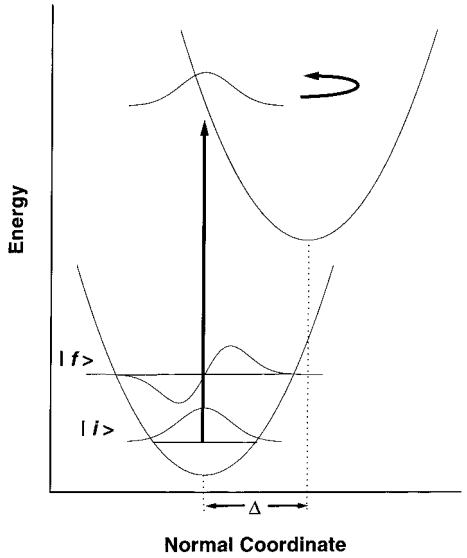

Figure 1. Wavepacket picture of absorption and resonance Raman scattering. For both processes, the incident photon carries the ground-state wave function to the excited electronic state potential energy surface where it propagates under the influence of the excited state Hamiltonian. For absorption, the overlap between this propagating wavepacket and the initial state is important; for resonance Raman, it is the overlap between this propagating wavepacket and the final state in the Raman process that is important.

The excited-state parameters of parsley plastocyanin have been obtained previously[6] by self-consistent analysis of the absorption spectrum and resonance Raman excitation profiles by using eqs 2 and 3. These parameters were used as a starting point in the analysis of spinach and poplar plastocyanin. For parsley plastocyanin, it was found that the absorption spectrum was completely homogeneously broadened, due to rapid population relaxation, dynamics, and protein-induced dephasing. The homogeneous lineshape function, $G(t)$, was found to

(16) Weiner, S. J.; Kollman, P. A.; Case, D. A.; Singh, U. C.; Ghio, C.; Alagona, G.; Profeta, S., Jr.; Weiner, P. *J. Am. Chem. Soc.* **1984**, *106*, 765.
(17) Weiner, S. J.; Kollman, P. A.; Nguyen, D. T.; Case, D. A. *J. Comput. Chem.* **1986**, *7*, 230.
(18) Aqvist, J.; Leijonmarck, M.; Tapia, O. *Eur. Biophys. J.* **1989**, *16*, 327.
(19) Levitt, M. *Annu. Rev. Biophys. Bioeng.* **1982,** *11*, 251.
(20) Makinen, M. W.; Troyer, J. M.; Van der Werff, H.; Berendsen, H. J. C.; Van Gunsteren, W. F. *J. Mol. Biol.* **1989**, *207*, 201.
(21) McCammon, J. A.; Wolynes, P. G.; Karplus, M. *Biochemistry* **1979**, *18*, 927.
(22) Gilson, M. K.; Sharp, K. A.; Honig, B. *J. Comput. Chem.* **1988**, *9*, 327.
(23) Jayaram, B.; Sharp, K. A.; Honig, B. *Biopolymers* **1989**, *28*, 975.
(24) Nicholls, A.; Honig. B. *J. Comput. Chem.* **1991**, *12*, 435.
(25) Laberge, M.; Vanderkooi, J. M.; Sharp, K. A. *J. Phys. Chem.* **1996**, *100*, 10793.
(26) Lee, S.-Y.; Heller, E. J. *J. Chem. Phys.* **1979**, *71*, 4777.
(27) Loppnow, G. R.; Mathies, R. A. *Biophys. J.* **1988**, *54*, 35.
(28) Markel, F.; Ferris, N. S.; Gould, I. R.; Myers, A. B. *J. Am. Chem. Soc.* **1992**, *114*, 6208.

have the following form:

$$G(t) = \exp\left\{-\left(\frac{\Gamma^2 t^2}{\hbar} + g(t)\right)\right\} \quad (4)$$

where Γ is the pure population relaxation term and $g(t) = g_R(t) + ig_I(t)$ is the protein-induced dephasing term where[6,28,29]

$$g_R(t) = (D^2/\Lambda^2)[\exp(-\Lambda t/\hbar) - 1 + \Lambda t/\hbar] \quad (5a)$$

$$g_I(t) = (D^2/2kT\Lambda)[1 - \exp(-\Lambda t/\hbar)] \quad (5b)$$

In these equations, D is the coupling strength between the electronic and solvation coordinates, and $\hbar/\Lambda$ is the characteristic time of the solvent modulation.[13,28−34] For parsley plastocyanin, it was determined that the protein-induced dephasing term was in the slow modulation limit where $D \gg \Lambda$ and the resulting line shape is Gaussian.[6]

For the analysis, the initial guesses for the displacements along each normal coordinate (Δ) were found from the relative resonance Raman vibrational intensities at 568.2 nm assuming the intensities were proportional to Δ^2 and with I_{376} scaled arbitrarily to 1.0. All eight observed fundamental vibrational modes were used in the time-dependent calculations. Other parameters were initially selected from the parsley plastocyanin excited-state parameters. The relative Δ values were scaled to give the experimentally observed absorption and resonance Raman excitation profile band widths. The homogeneous line width (Γ) was determined primarily by the absolute magnitudes of the resonance Raman excitation profiles. No inhomogeneous broadening in any of the plastocyanins, as determined by the absorption and resonance Raman excitation profile band shapes, was necessary to reproduce the observed spectral data. The transition moment (M) and the energy gap between potential surfaces (E_0) were determined by the magnitude and position of the absorption spectrum. The parameters were optimized iteratively until the calculated and experimental absorption spectrum and resonance Raman excitation profiles were in agreement.

Results

A comparison of the resonance Raman spectra of poplar and spinach plastocyanin is shown in Figure 2. The poplar plastocyanin resonance Raman spectrum is identical to the previously reported resonance Raman spectrum of pure poplar *a* plastocyanin.[35] The cacodylate vibrations, used as the intensity standard, are visible as a pair of bands centered at 603 and 638 cm^{-1}. Approximately six intense bands are observed between 350 and 500 cm^{-1} and have been previously assigned to normal modes involving the Cu−S stretch mixed with other internal coordinates,[35−38] primarily those of the cysteinate ligand, although the exact assignments are still controversial.[36] The moderately intense bands at 263 and 760 cm^{-1} have previously been assigned to the symmetric Cu−N stretch from the histidine ligand(s) and the C−S stretch of the cysteinate ligand, respectively.[36] The broad band centered at 824 cm^{-1} arises from combination and overtone transitions of the vibrations between 350 and 500 cm^{-1}. In our samples, the 824 cm^{-1} band also contains a contribution from the broad 825 cm^{-1} As═O stretch of the cacodylate internal standard.[39,40] Because of the imprecision in the intensity of bands in the 800−900 cm^{-1} region, they were not used in the resonance Raman intensity analysis.

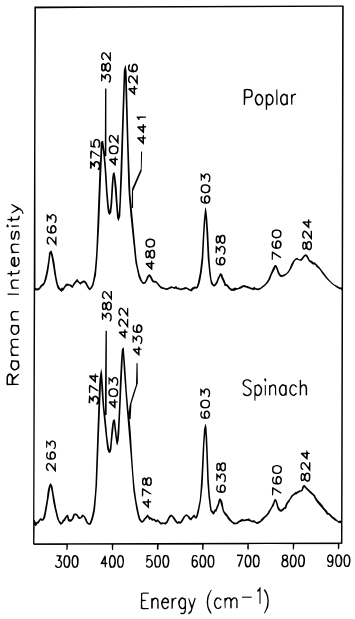

Figure 2. Resonance Raman spectra of 1 mM poplar *a* and spinach plastocyanin in 375 mM cacodylate buffer excited at 568 nm. The spectra are the sum of 3−9 scans and have been divided by a tungsten−halogen lamp spectrum. The cacodylate intensity standard vibrations appear at 603 and 638 cm^{-1}. The broad peak at 824 cm^{-1} is composed of the overtones and combination bands of the plastocyanin vibrations between 350 and 500 cm^{-1} as well as a broad cacodylate peak at 825 cm^{-1}. All of the indicated vibrations between 250 and 500 cm^{-1} and the vibration at 760 cm^{-1} were used in the analysis.

A comparison of poplar *a*, spinach, and parsley plastocyanin is shown for the 300−550 cm^{-1} spectral region in Figure 3. Note that many of the frequencies coincide within the ±2 cm^{-1} experimental error for spinach and poplar *a* plastocyanin. However, the modes at 426 (422) and 441 (436) cm^{-1} for poplar *a* (spinach) appear to have differences in frequencies that are real. More vibrations have significant differences when the resonance Raman spectrum of parsley plastocyanin is compared to those of the other two. A close examination of the spectra shows that there is a more obvious difference in the relative intensities of the vibrational bands from one species to the next. Significant differences in the relative intensities between the 375 and 382 cm^{-1} modes, 375 and 426 cm^{-1} modes, and 426 and 441 cm^{-1} modes in poplar *a* and spinach plastocyanin demonstrate that the mode-specific excited-state charge transfer dynamics are quite different in these two plastocyanins. Significant differences in the relative intensities between the 375 and 403 cm^{-1} modes, and 422 and 436 cm^{-1} modes in spinach and parsley plastocyanin, demonstrate that these proteins also have different mode-specific descriptions of their excited-state charge transfer dynamics.

Figures 4−6 illustrate the good agreement between the experimental and calculated resonance Raman excitation profiles and absorption spectra of spinach and poplar *a* plastocyanin

(29) Kulinowski, K.; Gould, I. R.; Myers, A. B. *J. Phys. Chem.* **1995**, *99*, 9017.
(30) Sue, J.; Yan, Y. J.; Mukamel, S. *J. Chem. Phys.* **1986**, *85*, 462.
(31) Bosma, W. B.; Yan, Y. J.; Mukamel, S. *Phys. Rev. A* **1990**, *42*, 6920.
(32) Mukamel, S. *Annu. Rev. Phys. Chem.* **1990**, *41*, 647.
(33) Loring, R. F.; Yan, Y. J.; Mukamel, S. *J. Chem. Phys.* **1987**, *87*, 5840.
(34) Yan, Y. J.; Mukamel, S. *J. Chem. Phys.* **1988**, *89*, 5160.
(35) Han, J.; Adman, E. T.; Beppu, T.; Codd, R.; Freeman, H. C.; Huq, L.; Loehr, T. M.; Sanders-Loehr, J. *Biochemistry* **1991**, *30*, 10904.
(36) Blair, D. F.; Campbell, G. W.; Schoonover, J. R.; Chan, S. I.; Gray, H. B.; Malmstrom, B. G.; Pecht, I.; Swanson, B. I.; Woodruff, W. H.; Cho, W. K.; English, A. M.; Fry, H. A.; Lum, V.; Norton, K. A. *J. Am. Chem. Soc.* **1985**, *107*, 5755.
(37) Woodruff, W. H.; Dyer, R. B.; Schoonover, J. R. In *Biological Applications of Raman Spectroscopy*; Spiro, T. G., Ed.; Wiley: New York, 1988; Vol. 3, p 413.
(38) Qiu, D.; Kilpatrick, L.; Kitajima, N.; Spiro, T. G. *J. Am. Chem. Soc.* **1994**, *116*, 2585.
(39) Grundler, H.-V.; Schumann, H. D.; Steger, E. *J. Mol. Struct.* **1974**, *21*, 149.
(40) Vansant, F. K.; van der Veken, B. J.; Herman, M. A. *Spectrochim. Acta, A* **1974**, *30A*, 69.

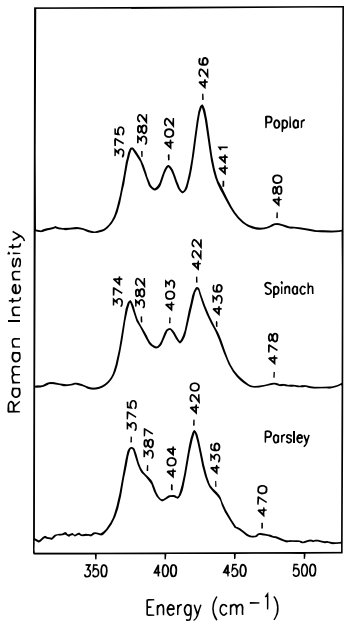

Figure 3. Resonance Raman spectra in the 300−525 cm^{-1} region of 1 mM poplar, spinach, and parsley plastocyanin in 375 mM cacodylate buffer excited at 568 nm. The spectra are the sum of 3−9 scans and have been divided by a tungsten−halogen lamp spectrum. Note the similar vibrational frequencies and significantly different relative intensities among the three spectra.

using the parameters summarized in Table 1. The experimental excitation profiles of the observed modes in all three species had similar shapes and, as observed before for parsley plastocyanin, are somewhat narrower than the absorption spectrum. These similarities in shape are borne out by the similarity in molecular excited-state parameters for the three species, particularly for those parameters that describe only the electronic characteristics of the excited state (e.g., transition dipole length and zero−zero energy). The absorption spectra of plastocyanin from the three species are superimposable, demonstrating that the electronic character of the excited charge transfer states is similar in the three plastocyanins. Also, the total absolute resonance Raman cross-sections, integrated over all of the observed vibrational bands, were the same within experimental error, indicating that the total charge transfer reorganization energy is similar for the three plastocyanins. The reorganization energies can be calculated from the values in Table 1 and from the relation $\lambda_{inner} = \Sigma(\Delta_i^2\omega_i)/2$, to yield total reorganization energies of 1480 cm^{-1} (0.18 eV), 1370 cm^{-1} (0.17 eV), and 1510 cm^{-1} (0.19 eV) for poplar *a*, spinach, and parsley plastocyanin, respectively. This similarity is reflected in the simulations (Table 1), in which identical homogeneous and inhomogeneous linewidths were used for the charge transfer excited state in the three species. Because the homogeneous linewidth contains contributions from the excited-state population relaxation and protein-induced dephasing rates, these results suggest that the kinetics of population relaxation and dephasing may be similar in the three species. However, to show definitively that the individual kinetics are similar, an independent measure of either the fluorescence quantum yield or dephasing rate, as has been done for parsley plastocyanin,[6] would have to be performed.

As illustrated in Figure 3, however, the relative resonance Raman intensities vary with species. This modulation in the mode-specific description of charge transfer is directly reflected in the different experimental absolute resonance Raman cross-sections (Figures 4 and 5) and excited-state geometry displacements (Table 1) in the three species for the same vibrational band (e.g., compare the excitation profiles for the 426 cm^{-1} mode of poplar *a* and the 422 cm^{-1} mode of spinach plastocyanin in Figures 4 and 5). This difference is illustrated more clearly in Table 1, which presents the excited-state parameters as a function of the species of plant from which the plastocyanin is obtained This table shows that all of the excited-state parameters, except for the weak modes at ∼480 and ∼760 cm^{-1}, are significantly different in the three plastocyanins (i.e., no intense mode provides a useful internal intensity standard by which to judge the relative intensity changes in this region of the spectrum). However, there are a few trends which are clearly derived from Table 1. Qualitatively, the changes in relative intensity shown in Figure 3 are reflected in the excited-state displacement comparison of Table 1. Comparing poplar *a* and spinach plastocyanin, the excited-state displacement, Δ, of the 382 cm^{-1} mode is larger in poplar *a* than in spinach plastocyanin, while the Δ of the 375 cm^{-1} mode is nearly identical in the two species. The Δ of the 426 cm^{-1} mode is significantly larger and the Δ of the 441 cm^{-1} mode is significantly smaller in poplar *a* than in spinach plastocyanin. In parsley plastocyanin, the excited-state displacements in all the modes are different from the displacements in the other two plastocyanins. The Δ values of both the 375 and 387 cm^{-1} modes are significantly higher than the Δ values of the same modes in spinach and poplar *a* plastocyanin. The Δ of the 404 cm^{-1} mode is smaller than the Δ of the same mode in the other plastocyanins by almost a factor of 2. The Δ values of the 420 and 436 cm^{-1} modes are about the average of the Δ values for the same modes in the other two plastocyanins. The molecular origin of these intensity redistributions, particularly in spinach and poplar *a* plastocyanin, will be discussed below.

Discussion

The primary purpose of this paper is to explore the role of solvent on excited-state charge transfer dynamics by using a structurally well-defined solute and solvent, in this case the blue copper protein plastocyanin from parsley, spinach, and poplar. The resonance Raman data presented here indicate many similarities, but some significant differences, in the excited state structure and dynamics of these three plastocyanins. Clearly, many of the electronic characteristics of the charge transfer excited-state in the three plastocyanins are similar or identical. This conclusion is a result of the almost superimposable absorption spectra and the identical values of the transition moment, homogeneous linewidth, inhomogeneous linewidth, and zero−zero energy obtained from the self-consistent analysis of the absorption spectra and resonance Raman excitation profiles. The vibrational characteristics also exhibit clear and significant differences in the resonance Raman intensities (and resulting Δ values from the self-consistent analysis) and very small shifts in the frequencies of some of the resonance-enhanced vibrations.

To understand the molecular origin of these observed spectral differences, we have performed a detailed comparison of the structure and electrostatic potential in spinach and poplar *a* plastocyanin. These two proteins provide the best comparison because they have the highest sequence homology of the three possible pairs, with a different amino acid in only 22 of the 99 positions (78% homologous, Table 2).[15] Of the differences, nine are considered conservative, with substitutions such as a valine for a leucine, a glutamate for an aspartate, or a tyrosine for a phenylalanine. Also, the X-ray crystal structure has been determined for poplar *a* plastocyanin, providing at least a starting point for some structural comparisons of the two plastocyanins.[13] Finally, the plastocyanins from these two species exhibit the

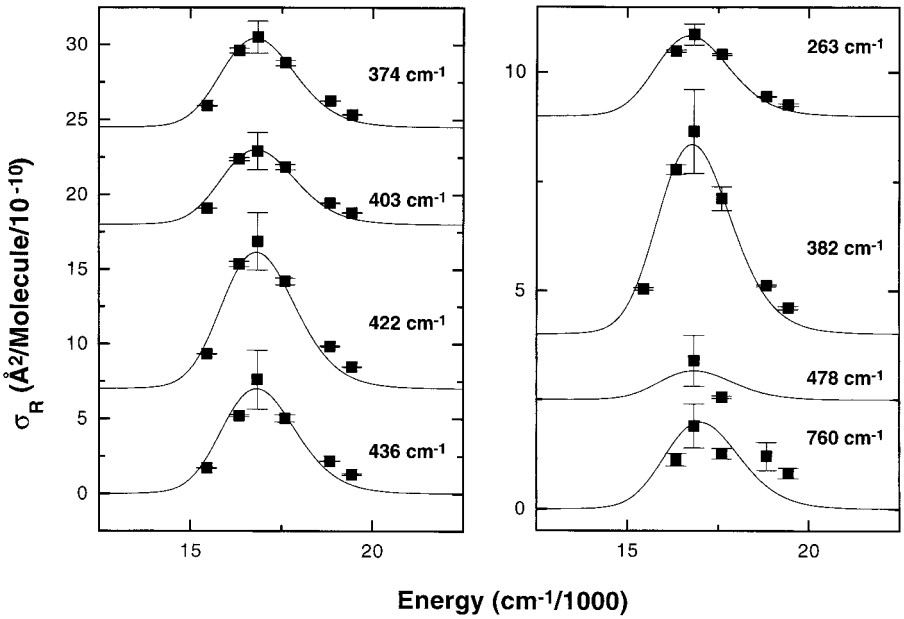

Figure 4. Experimental (points) and calculated (solid line) resonance Raman excitation profiles of spinach plastocyanin. The excitation profiles were calculated with eq 3 by using the parameters of Table 1. Error bars represent the uncertainties in the absolute resonance Raman cross-sections. Note the difference in *y*-axis scales between the left and right panels.

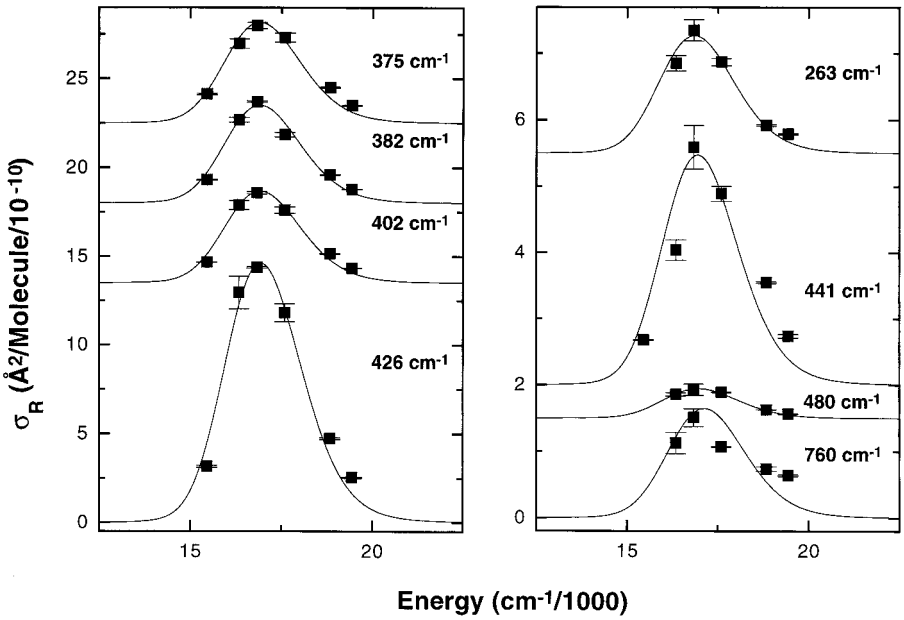

Figure 5. Same as Figure 4, but for poplar *a* plastocyanin.

most similar resonance Raman vibrational frequencies of the three possible pairs, but show significant differences in relative resonance Raman intensity and excited state displacements. Thus, the remainder of the comparison will focus on these two plastocyanins.

A close examination of the structure of poplar *a* plastocyanin[13] and a detailed comparison of the amino acid sequence for poplar *a* and spinach plastocyanins[15] indicate that most of the differences in the primary structure lie far from the Cu site; the closest residue substitution to the copper site is Ile_{39} (Val_{39} in spinach plastocyanin) at a distance of 7.8 Å. The other residues all lie more than 10 Å away from the Cu site. In addition, the side chains of all the differing amino acids but two stick into the outside solvent, rather than into the interior of the protein. Thus, these residues probably have less influence on the structure of the copper site than the interior amino acids. The two interior amino acids are Ile_{21} and Ile_{39} in poplar *a* plastocyanin which become Val_{21} and Val_{39}, respectively, in spinach plastocyanin. The conservative nature of these substitutions suggests that their effect on the electrostatic environment and structure at the Cu site will be minimal.

To quantitate the significance of these amino acid variances on the structure of the copper site, molecular modeling calculations were performed on spinach and poplar *a* plastocyanin. As pointed out above, the resonance Raman frequencies, with two possible exceptions, are similar for spinach and poplar *a* plastocyanin. This similarity suggests these two plastocyanins exhibit minimal changes in ground-state structure, although the existence of several resonance Raman-enhanced modes at nearly identical frequencies in this protein may make a definitive statement of the involvement of ground-state structural changes difficult. In addition, the presence of resonance-enhanced modes with slight frequency shifts suggests that the normal mode description of the vibrations may be different in the two plastocyanins. To examine the role of any ground-state structure change in the observed resonance Raman frequencies and

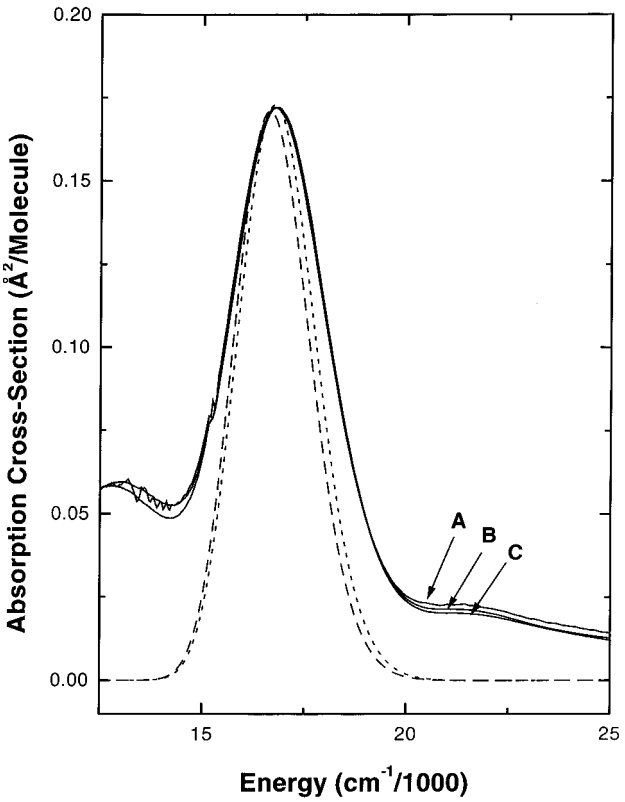

Figure 6. Experimental (solid lines) and calculated (dashed/dotted lines) absorption spectra of plastocyanin. Experimental spectra are shown for spinach (A), poplar *a* (B), and parsley (C) plastocyanin. Calculated spectra are shown for spinach (dashed) and poplar *a* (dotted) plastocyanin. The dashed and dotted lines are generated from eq 2 by using the parameters of Table 1. Deviations of the calculated from the experimental absorption spectrum at higher and lower energies arise from other electronic transitions that were not modeled and that apparently contribute no resonance enhancement to the observed resonance Raman spectra.

Table 1. Harmonic Mode Parameters of Poplar *a*, Spinach, and Parsley Plastocyanin[a]

poplar *a*		spinach		parsley	
mode (cm^{-1})	$\|\Delta\|$	mode (cm^{-1})	$\|\Delta\|$	mode (cm^{-1})	$\|\Delta\|$
263	0.87	263	0.89	266	0.98
375	1.13	374	1.14	375	1.35
382	1.08	382	0.96	387	1.20
402	1.00	403	0.98	404	0.49
426	1.59	422	1.26	420	1.44
441	0.75	436	1.07	436	0.98
480	0.25	478	0.30	470	0.24
760	0.31	760	0.34	759	0.35

[a] Δ values are in units of dimensionless normal coordinates. For all species, the calculations used temperature $T = 0$ K, Gaussian homogeneous linewidth $\Gamma = 385$ cm^{-1}, and no inhomogeneous broadening. For poplar *a* and parsley[6] plastocyanin, $E_0 = 15350$ cm^{-1} and transition length $M = 0.58$ Å. For spinach plastocyanin, $E_0 = 15500$ cm^{-1} and transition length $M = 0.57$ Å. The estimated errors in the parameters used in the calculation are as follows: zero−zero energy (E_0), ±1%; transition length (M), ±1%; homogeneous linewidth, ±5%; displacements, ±10%.

intensities, we compared the minimized experimentally-determined poplar *a* and the minimized computationally-derived spinach plastocyanin structures (Figures 7 and 8). As these figures show, the structural differences localized at the copper site and within the immediate coordination sphere are minimal. However, these figures show increasingly greater structural differences as the peptide chain is followed from the copper site toward the closest amino acid residue difference in the two

Table 2. Amino Acid Differences in Spinach and Poplar *a* Plastocyanin[a]

position	poplar *a*	spinach	conservative?	structural?	electrostatic (poplar *a*/spinach)
1	Ile	Val	Y	N	0/0
2	Asp	Glu	Y	N	−/−
7	Ala	Gly	Y	N	0/0
8	Asp	Gly	N	N	−/0
15	Val	Leu	Y	N	0/0
17	Ser	Gly	N	N	polar/0
18	Glu	Asp	Y	N	−/−
21	Ile	Val	Y	Y	0/0
22	Ser	Ala	N	N	polar/0
23	Pro	Ser	N	Y	0/polar
26	Lys	Glu	N	N	+/−
39	Ile	Val	Y	Y	0/0
45	Ser	Glu	N	N	polar/−
53	Ser	Ala	N	N	polar/0
66	Lys	Pro	N	Y	+/0
70	Phe	Tyr	Y	N	0/polar
71	Glu	Lys	N	N	−/+
73	Ala	Thr	N	N	0/polar
75	Ser	Thr	Y	N	polar/polar
76	Asn	Glu	N	N	polar/−
79	Glu	Thr	N	N	−/polar
81	Ser	Lys	N	N	polar/+

[a] Sequences are taken from ref 15. Conservative refers to whether the general properties of the side chains of the two amino acids are similar. Structural differences are those that introduce possible structural changes in the protein, with the most significant being a proline substitution and those amino acid side chains that are buried in the interior of the protein. "Y" and "N" refer to "yes" and "no", respectively. Electrostatic differences are those that result in significantly different charge or polarity properties in the two amino acid side chains at the pH used. Here, "0" means uncharged and nonpolar, "+" means positively charged, "−" means negatively charged, and "polar" means uncharged and polar.

plastocyanins. Past descriptions of the normal mode structure at the copper site emphasized local considerations, extending at most to the amino acids involved in the immediate coordination sphere.[35−38,41] If these normal mode descriptions were accurate, the results of the protein minimization suggest that no change in either the observed frequencies or intensities would occur between spinach and poplar *a* plastocyanin. Because of the observed spectroscopic differences, we suggest here that those normal mode descriptions may be incomplete, and that the protein may contribute remote internal coordinates to the normal modes resonantly enhanced within the 597 nm charge transfer absorption band.

In addition to modeling the ground-state structure of the two plastocyanins, calculations of the electrostatic potentials within the proteins were performed to examine the role of the environment on the charge transfer dynamics. The absorption spectra of the three plastocyanins exhibit identical absorption maxima, band shapes, band widths, and extinction coefficients, indicating that the electronic structure is similar. In addition, the total reorganization energy in the three plastocyanins upon excited state charge transfer, the zero−zero energy, and the transition dipole moment are the same within experimental error. These results suggest that the electrostatic environment is not significantly different at the copper sites in the two plastocyanins. This is confirmed in the electrostatic potential calculations on the poplar *a* and derived spinach plastocyanin structures (Figures 9 and 10). These calculations show that the copper ion sits in a region of high positive electrostatic potential and that this potential is identical in the two plastocyanins. How-

(41) Qiu, D.; Dong, S.; Ybe, J. A.; Hecht, M. H.; Spiro, T. G. *J. Am. Chem. Soc.* **1995**, *117*, 6443.

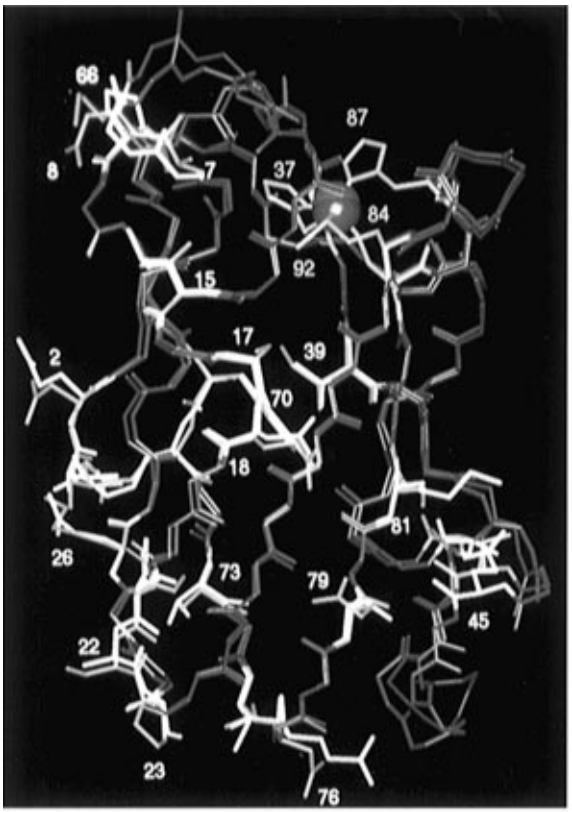

Figure 7. Comparison of the backbone structures of minimized poplar *a* (blue) and spinach (red) plastocyanin. The copper ion of each is rendered as CPK type. For reference, the copper ligands, His37, Cys84, His87, and Met92, are shown in light blue and labeled. The side chains of only the differing amino acids are shown for poplar *a* (green) and spinach (white) plastocyanins. Most of these different amino acids have been labeled with the residue number for reference. Note the similarity in backbone structure near the copper site and the small substitution at residue 39, the amino acid difference closest to the copper site.

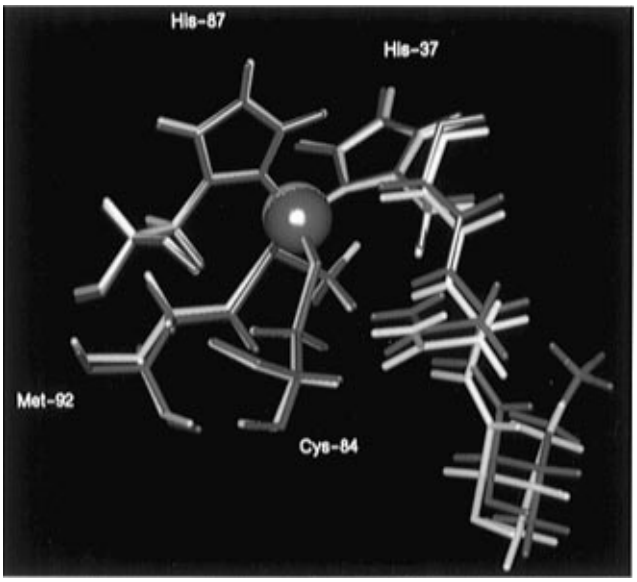

Figure 8. Copper site structure of minimized poplar *a* (blue) and spinach (light green) plastocyanins. The immediate coordination ligands are shown, as well as amino acids 38 and 39. The additional methyl group on amino acid residue 39 in poplar *a* plastocyanin is highlighted in red. Note that both plastocyanins have identical copper site structures, extending to the immediate coordinating amino acid side chains.

ever, the electrostatic potential around the periphery of the protein is different in the two plastocyanins, reflecting the nonconservative changes in charged amino acid residues in this region. These changes in electrostatic potential at the periphery of the protein may be responsible for the altered intermolecular interactions that allow poplar *a* plastocyanin to crystallize while preventing spinach plastocyanin from forming good crystals.[13] Thus, it is not surprising that the electronic structure at the copper site in all three plastocyanins is very similar and suggests that, on the molecular scale, remote charge effects (i.e., at distances ≥ 10 Å) in plastocyanins may not play a significant role in mediating electron transfer.

The modeling of plastocyanin presented here suggests that neither the ground-state structure nor the electrostatic potential is different in the two plastocyanins. However, the differences observed in the resonance Raman spectra of poplar *a* and spinach plastocyanin remain to be explained in a molecular context. The observed changes in Δ values along the various modes may arise from two possible sources: (1) the ground-state or excited state equilibrium geometry along each normal coordinate may shift as a result of protein composition, with the same normal coordinate descriptions for spinach and poplar *a* plastocyanin, or (2) the normal mode description may change as a function of protein composition due to differences in ground-state equilibrium geometries and/or conformation-dependent changes in coupling. There is some experimental evidence for both of these mechanisms and both will be discussed in detail below.

The first mechanism is simply a change in the displacement along one or more normal coordinates, without any change in the normal mode description. This mechanism may be visualized as a change in the potential interactions in the excited state with a change in the protein composition. For example, the presence of a new amino acid side chain in a spatial position within the protein close to the motion of the distorting copper site after absorption of a photon would introduce a new repulsive interaction on the excited state potential energy surface, and this could lead to a change in the equilibrium geometry configuration in the excited state, yielding a different value for Δ. This new interaction, either repulsive or attractive, may not change the ground-state geometry or the normal mode description if it occurs at a significant distance from the copper site. Such an interaction would be expected to change the Δ values of the different normal modes independently, depending on the spatial proximity of the distorting normal coordinate to the new interaction. Our resonance Raman results show that the total resonance Raman intensity from 300−525 cm^{-1} is conserved in the different plastocyanins, suggesting that the intensity is being redistributed among the normal modes upon changes in the protein composition, rather than increasing or decreasing. Sanders-Loehr and co-workers have suggested that the intensity in the resonance Raman spectrum arises from the Cu−S stretching internal coordinate alone.[42,43] It is difficult to imagine a mechanism in which the equilibrium Cu−S bond length is affected differently in two normal modes as a result of a new repulsive or attractive interaction.

It is much more reasonable to suggest that the redistribution of resonance Raman intensity arises from a change in the normal mode description in the two proteins as a result of the change in amino acid composition. This change in normal mode description may be caused by a difference in ground-state equilibrium geometries and/or conformation-dependent changes in coupling among the internal coordinates which make up the normal modes. The difference hinges on whether the ground-

(42) Han, J.; Loehr, T. M.; Lu, Y.; Valentine, J. S.; Averill, B. A.; Sanders-Loehr, J. *J. Am. Chem. Soc.* **1993**, *115*, 4256.

(43) Andrew, C. R.; Yeom, H.; Valentine, J. S.; Karlsson, B. G.; Bonander, N.; van Pouderoyen, G.; Canters, G. W.; Loehr, T. M.; Sanders-Loehr, J. *J. Am. Chem. Soc.* **1994**, *116*, 11489.

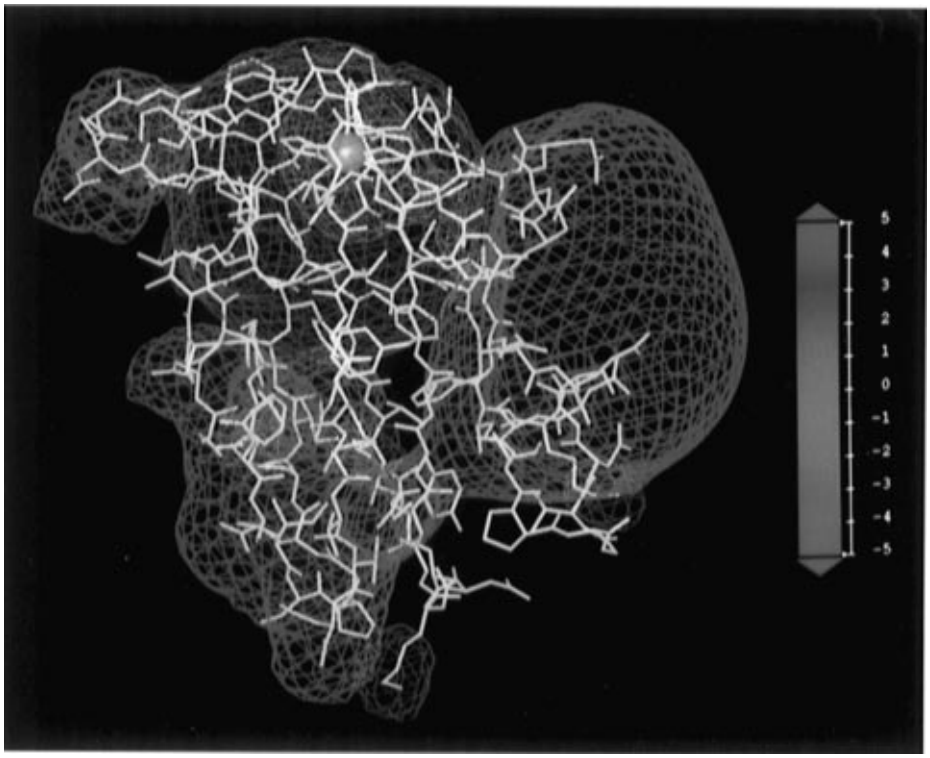

Figure 9. Electrostatic potential contour diagram of poplar *a* plastocyanin from the finite difference method of solving the linear Poisson−Boltzmann equation. Contours of negative potential are shown in red and positive potential in blue, with the scale on the right in units of kT (1 kT = 0.592 kcal/mol). The copper ion is shown in light blue and sits in a site of high positive potential.

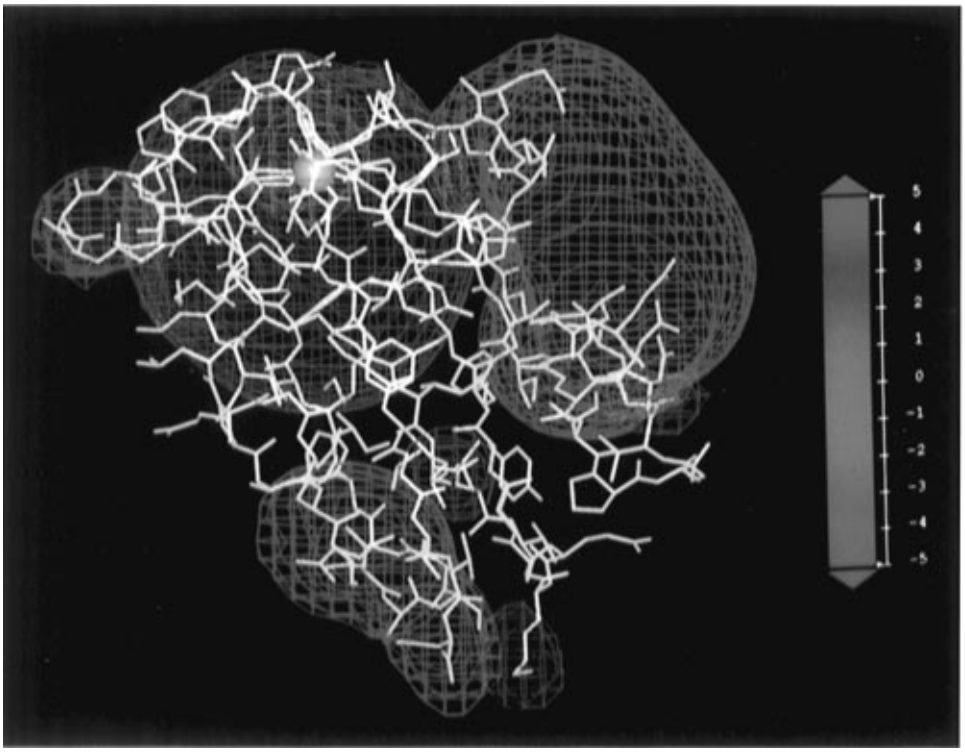

Figure 10. Same as Figure 10, but for spinach plastocyanin.

state equilibrium structure at the copper site (including all the important internal coordinates making up the resonance-enhanced normal modes) is the same in the two plastocyanins. The molecular modeling results of Figures 7 and 8 suggest the ground-state structure is similar for these two plastocyanins. The slight frequency shifts observed for the two modes whose intensities change the most between spinach and poplar *a* plastocyanin support the idea that the normal mode description may be different. This change in the normal mode description can be thought of as a rotation of both the ground- and excited-state potential energy surfaces as a function of the protein composition. Since the ground-state equilibrium geometry appears to be similar in the two proteins, the rotation would occur around the ground-state equilibrium geometry. In plastocyanin, the change in the normal mode description appears to affect only two modes, as judged by the intensity and frequency changes, the 426 and 441 cm^{-1} modes. Because these two modes appear at essentially the same frequency, rotation

of the normal modes will have minimal effect on the frequencies, but can significantly change the intensity distributed among the two normal modes involved. *Since this normal mode description change does not appear to be the result of any equilibrium structural change, the internal coordinates of the protein, far from the copper site, must be directly coupled into the resonance-enhanced modes at the copper site. This suggests a long-range coupling in plastocyanins, important for dictating the coordination geometry at the copper site and, therefore, its redox potential.* It is important to note that, although internal coordinates far from the protein may be coupled into the resonance-enhanced normal modes at the copper site, they may not undergo any distortion upon excitation to the charge transfer excited state (i.e., the intensity of the normal mode may still derive from changes in internal coordinates localized at the copper site, such as the Cu−S stretch).

Such long-range coupling has been predicted from normal mode calculations[44] and molecular dynamics simulations.[45] The normal mode calculation,[44] based on a 169-atom subset of poplar *a* plastocyanin, predicted internal coordinates from most amino acid residues within a ∼10 Å radius around the copper site to be involved in the resonance-enhanced normal modes at ca. 400 cm^{-1}. The molecular dynamics simulation[45] correlated protein atomic motions with the Cu−S bond length change from the calculated ground-state and charge transfer excited state potential energy surfaces. This latter study found that motions of residues 83−87, the proposed electron transport pathway, were the most highly correlated with the Cu-S bond length changes. The resonance Raman spectra and molecular modeling results reported here represent the first experimental test of these predictions and are in qualitative agreement with them. However, the results presented here suggest that other protein motions than those identified in the simulations reported above may be at least as important in the excited-state charge transfer dynamics of plastocyanin.

(44) Urushiyama, A.; Tobari, J. *Bull. Chem. Soc. Jpn.* **1990**, *63*, 1563.
(45) Unger, L. W.; Scherer, N. F.; Voth, G. A. *Biophys. J.* in press.

Conclusions

The coupling of protein internal coordinates at a distance of ≥8 Å from the copper site to normal coordinates resonance-enhanced by an electronic transition localized at the copper site in plastocyanin, a blue copper protein involved in photosynthetic electron transport, has been proposed here by comparing the resonance Raman-derived excited-state dynamics in three plastocyanins with slightly different amino acid composition. A comparison of the structure and electrostatic potential in these plastocyanins from molecular modeling suggests that the different mode-specific dynamics observed are the result of different normal mode descriptions of the resonance-enhanced vibrations in the different proteins. These results imply that a significant portion of the protein, which is not directly involved in binding of redox partners, appears to be involved in determining the coordination geometry and redox potential at the copper site. These results provide insight into the methods nature uses to construct appropriate active sites in proteins.

Acknowledgment. The authors thank J. Lee for help in the purification of spinach and poplar plastocyanins and M. Palcic, H. B. Dunford, D. Bundle, and N. Dovichi for the use of equipment. The authors also thank N. Scherer for providing preprints of his work and S. Nilar for helpful discussions. Financial support was provided by NSERC and the Alberta Heritage Foundation for Medical Research.

Supporting Information Available: Figures 11 and 12 showing the resonance Raman spectra of spinach and poplar *a* plastocyanin at the excitation wavelengths used in this study and Tables 3 and 4 listing the experimental and calculated absolute resonance Raman cross-sections for spinach and poplar *a* plastocyanin for each observed mode at each excitation wavelength (5 pages). See any current masthead page for ordering and Internet access instructions.

JA962983Z